



The preparation and photocatalytic activity of phosphotungstic acid-reduced graphene oxide composites

Li-hong Xia^a, Li-jun Luo^{a,*}, Junhong Li^a, Ya Fan^a, Wei Tan^a, Wen-rong Yang^b,
Hong-bin Wang^{a,*}, Li Shu^c

^aKey Laboratory of Resource Clean Conversion in Ethnic Regions, Education Department of Yunnan, School of Chemistry and Environment, Yunnan MinZu University, Kunming 650500, China, emails: 10501931@qq.com (L. Luo), 1339953681@qq.com (L. Xia), 790555069@qq.com (J. Li), 1416655459@qq.com (Y. Fan), 317366182@qq.com (W. Tan), 595530820@qq.com (H. Wang)

^bCentre for Chemistry and Biotechnology, School of Life and Environmental Sciences, Deakin University, Waurn Ponds, VIC 3216, Australia, email: wenrong.yang@deakin.edu.au

^cSchool of Civil, Environmental and Chemical Engineering RMIT University, Melbourne, VIC 3000, Australia, email: li.shu846@gmail.com

Received 9 June 2017; Accepted 11 September 2017

ABSTRACT

In this work, phosphotungstic acid-reduced graphene oxide composites (denoted as HPW-RGO) were synthesized using phosphotungstic acid and self-made graphene oxide as starting materials via a facile hydrothermal method. The prepared materials were characterized by scanning electron microscopy, X-ray diffraction analysis, infrared spectroscopy, X-ray photoelectron spectroscopy and thermogravimetric analysis. The results showed that the phosphotungstic acid particles were loaded on reduced graphene oxide. The optimal mass ratio of graphite oxide to HPW was 3.0 wt% in preparation process. Under the same experimental condition (pH 3.0, 20 mg/L methyl orange (MO) and 1.0 g/L dosage), the adsorption removal ratio of MO over HPW-3RGO was 46.34%, the photocatalytic degradation removal ratio is about 40.00%, and the total removal ratio was 86.34%. While the adsorption removal ratio of MO over HPW was only 2.67%, the photocatalytic degradation removal ratio is about 32.00% and the total removal ratio was only 34.66%. The degradation rate constant of HPW-3RGO (0.00892 min^{-1}) was 3.4 times of the HPW (0.00264 min^{-1}).

Keywords: Photocatalysis; Phosphotungstic acid; Graphene; Methyl orange

1. Introduction

Photocatalytic technique has attracted much attention because it is considered to be a promising way to challenge the worldwide energy shortage and environmental pollution issues. It can mineralize environmental pollutants under solar light completely. Titanium dioxide (TiO_2) is the commonly used photocatalyst because it has good virtues, such

as high photocatalytic efficiency, chemical inertness, photostability, low cost and nontoxicity [1,2]. However, there are some drawbacks including its wide band gap (3.2 eV), fast recombination of the photo-generated electron-hole pairs and low adsorption ability for pollutants. Such disadvantages restricted the large-scale industrial application of TiO_2 in real wastewater treatment. Therefore, it is important and necessary to explore new efficient photocatalyst to meet these needs.

* Corresponding author.

Presented at the 9th International Conference on Challenges in Environmental Science & Engineering (CESE-2016), 6–10 November 2016, Kaohsiung, Taiwan, 2016

Recently, polyoxometalates have attracted particular interest in photocatalysis field due to their strong Brønsted acidity. However, one of the major disadvantage is relative low photocatalytic activity because of the combination of photo-generated electron–hole pairs and small surface area. In order to overcome this disadvantage, the heteropolyacids have been anchored on the supporters, such as zeolites [3], activated carbon [4], mesoporous silica [5,6] and TiO_2 [7]. Another method was that heteropolyacid precipitated with K^+ , NH_4^+ [8,9], La^{3+} and Ce^{3+} [10] to form salts with higher photocatalytic activity.

Graphene, a single atomic layer of sp^2 -hybridized carbon arranged in a honeycomb structure, is the 2D allotrope of carbon [11]. Since 2009, it has drawn enormous scientific attention because of its high specific surface area [12], excellent conductivity [13] and good adsorption ability for organic pollutants [14]. Up to date, many works about the graphene-based photocatalysts to decompose organic pollutants [15,16] or split water to produce hydrogen [17,18] have been reported.

In this work, in order to improve the adsorption and photocatalytic performance of phosphotungstic acid, RGO as a supporter was introduced to phosphotungstic acid to obtain HPW-RGO composites. The morphology, crystal phase structure and chemical composition of the HPW-RGO composites were investigated in detail. The adsorption and photocatalytic performance of them were evaluated by removing MO as model pollutant. Moreover, the mass ratio of graphite oxide to HPW was optimized during the preparation process.

2. Experiments and methods

2.1. Chemicals and materials

Flake graphite powder (325 mesh) was supplied by Qingdao Henglid Graphite Co., Ltd. (China). Potassium permanganate (KMnO_4), sodium nitrate (NaNO_3), H_2SO_4 (98%) and hydrogen peroxide (H_2O_2 , 25%) were purchased from Chengdu Kelong Chemical Reagent Factory (China). Phosphotungstic acid ($\text{H}_3\text{PW}_{12}\text{O}_{40}\cdot x\text{H}_2\text{O}$) and methyl orange (MO) were bought from Sinopharm Chemical Reagent Co., Ltd. (China). All the reagents were analytical grade and were used as received. Ultra-pure water (18.2 M) used throughout the experiments was obtained from laboratory purification system.

2.2. Synthesis of HPW-RGO composites

Graphite oxide was prepared using natural flake graphite powder (325 mesh) through a modified Hummers method [19,20]. In total, 2 mg/mL of graphene oxide (GO) was obtained by ultrasonic treatment, the experiment process was following: 0.6 g of graphite oxide was added into 300 mL of mixture solvent [water–ethanol (2:1)], then above suspension was sonicated for 6 h and centrifuged at 4,000 rpm for 15 min. The supernatant (GO) was collected and kept in a refrigerator for latter usage. Phosphotungstic acid-reduced oxide graphene composites (denoted as HPW-RGO) were synthesized using 2 mg/mL GO solutions and phosphotungstic acid as starting materials via simple hydrothermal method, which was similar to Zhang et al. [15] and Zhang et al. [21] works.

The HPW-RGO composites with different RGO contents (1, 3 and 5 wt%) were prepared by adjusting the mass ratios of graphite oxide to HPW, and products were denoted as HPW-1RGO, HPW-3RGO and HPW-5RGO. In a typical preparation process of HPW-3RGO composite, 1 g of $\text{H}_3\text{PW}_{12}\text{O}_{40}\cdot x\text{H}_2\text{O}$ was added into mixture solution containing 15.00 mL of 2 mg/mL GO solution under stirring, further stirred for 2 h, and then the suspension was transferred into a 25-mL teflon-sealed autoclave for hydrothermal treatment at 120°C for 8 h. Finally, the resulting composite was dried at 50°C in vacuum. The RGO was prepared with the same method only without adding HPW during preparation process.

2.3. Characterization of HPW/RGO composites

SEM images were captured on an FEI QUANTA200 scanning electron microscope (USA). The crystal phase structure of prepared materials were recorded on a TTRIII diffractometer (Rigaku Corporation, Japan) with $\text{Cu K}\alpha$ radiation in the 2θ range from 5° to 70°. The scanning rate was 10° min^{-1} and a step size was 0.02° s^{-1} , the accelerating voltage and the applied current were 40 kV and 30 mA, respectively. Fourier-transform infrared spectra (FTIR) were conducted on a Nicolet iS10 FTIR Spectrometer (Thermo Scientific, Germany) using KBr pellet technique over the wave number range of 4,000–400 cm^{-1} with a resolution of 2 cm^{-1} . X-ray photoelectron spectrum (XPS) measurements were performed on a PHI5000 Versaprobe scanning XPS microprobe (ϕ ULVAC-PHI Inc.) using the $\text{Al K}\alpha$ line. For calibration purposes, the main C1s peak was referenced to 284.8 eV. The thermal stability of prepared materials were also measured on a thermal gravimetric analyzer (TGA, NETZCH, TG209FI, Germany), the heated temperature were from room temperature to 700°C at 20°C min^{-1} heat rate.

2.4. Evaluation of performance of materials

Photocatalytic degradation experiments were performed in XPA-7 photochemical reactor (Xujiang Electromechanical Plant, Nanjing, China) to investigate adsorption and photocatalytic degradation removal of MO. The light is 20 W UV lamp ($\lambda = 254$ nm). The reaction suspensions were cooled by circulating water at room temperature. In a typical experimental process, 0.0500 g of HPW-RGO was added into 50 mL of MO solution (C_0). Prior to the light irradiation, the suspensions were stirred in dark for 120 min to establish the adsorption/desorption equilibrium and the MO concentration was determined as C_q (adsorption/desorption equilibrium time is about 20 min, in order to meet adsorption equilibrium, the suspension was stirred in dark for 120 min). Then irradiation started and a quartz tubes containing 50 mL of MO solution were taken out at scheduled time and its concentration was determined as C_t . The suspension solution was immediately filtered through a 0.45- μm glass fiber filter to remove the catalyst particles and subjected to ultraviolet–visible spectrum analysis (detection wavelength was 463 nm), the standard curve for MO was linearly best fitted ($R^2 = 0.9999$) with the concentration of MO varied from 1 to 20 mg/L.

The adsorption and photocatalytic degradation removal ratios of MO on photocatalysts were calculated according to Eq. (1) and Eq. (2), respectively.

$$\text{Removal ratio by adsorption (\%)} = \frac{C_0 - C_q}{C_0} \times 100\% \quad (1)$$

Removal ratio by photocatalytic

$$\text{degradation (\%)} = \frac{C_0 - C_t}{C_0} \times 100\% \quad (2)$$

In order to further compare the photocatalytic performance of HPW-RGO with that of pure HPW, the experimental data were fitted by pseudo-first-order model. Its equation can be written in a linear form and shown in Eq. (3):

$$\ln \frac{C_t}{C_0} = -\kappa t \quad (3)$$

The slope of the fitted line of $\ln(C_t/C_0)$ vs. reaction time was the rate constant (κ).

3. Results and discussion

3.1. Characterization of HPW-RGO composites

3.1.1. Morphology

To observe the morphology of the as-synthesized composites, the SEM images of GO, HPW and HPW-3RGO are shown in Fig. 1. It can be seen that bare GO (Fig. 1(a)) had a flake-like structure with wrinkles and the HPW was the block with cracks, and HPW-3RGO composite showed that HPW particles were well-dispersed and loaded on the RGO sheets without obvious aggregation. This result can improve the adsorption and photocatalytic activity of HPW.

3.1.2. Crystal phase structure

In order to investigate the crystal phase of as-synthesized GO, RGO, HPW-1RGO, HPW-3RGO and HPW-5RGO, the X-ray diffraction (XRD) patterns of them were recorded on a TTRIII diffractometer. Fig. 2 illustrates that GO had a sharp and strong characteristic peak at $2\theta = 10.8^\circ$, the diffraction peak of GO disappeared at $2\theta = 10.8^\circ$ and a new characteristic peak of RGO at $2\theta = 24.5^\circ$ appeared after hydrothermal reduction in the solvent of ethanol–water (1:2). This result implied that the GO may be reduced to RGO when ethanol was as a reductant in hydrothermal environment [22]. The XRD patterns of HPW showed that it is well crystallized, and HPW had peaks at 10.3° , 14.6° , 17.9° , 20.5° , 23.2° , 25.3° , 29.6° , 34.4° , 37.9° , 53.4° and 60.0° , which are the characteristic peaks of HPW [3]. Fig. 3 was the XRD patterns of HPW, HPW-1RGO, HPW-2RGO and HPW-3RGO, the XRD patterns of them were similar with the XRD pattern of HPW, and no obvious RGO peaks were observed because of weak intensity of RGO possibly. Moreover, with the increasing of RGO mass ratio from 1 to 5 wt% in HPW-RGO composites, the intensity of diffraction peaks of HPW at 10.3° and 25.3° became weaker, which could be ascribed to the shielding effect of RGO on the HPW surface. Therefore, the higher mass ratio of RGO in composite maybe made weak absorption for ultraviolet because of shielding effect of RGO for light, which will lead to weak photocatalytic degradation performance for target pollutants.

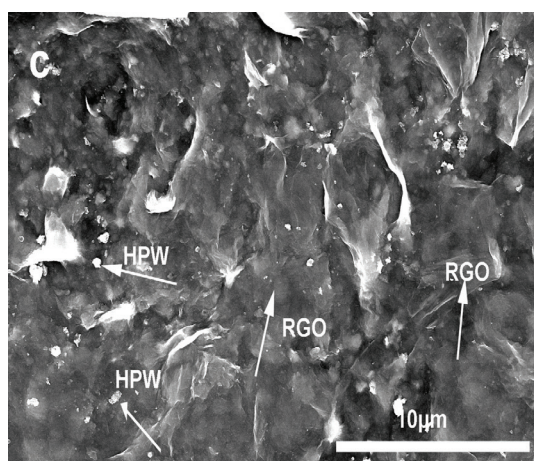
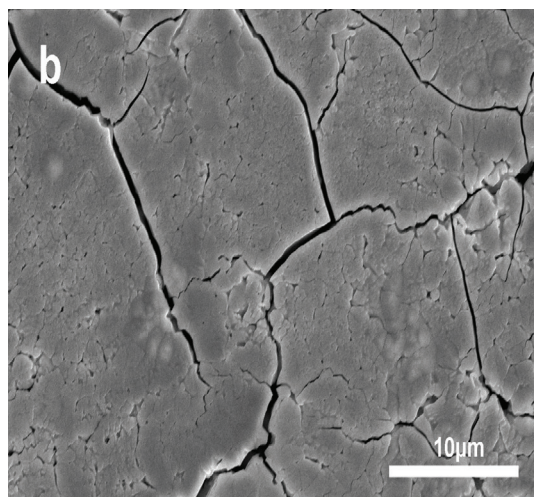
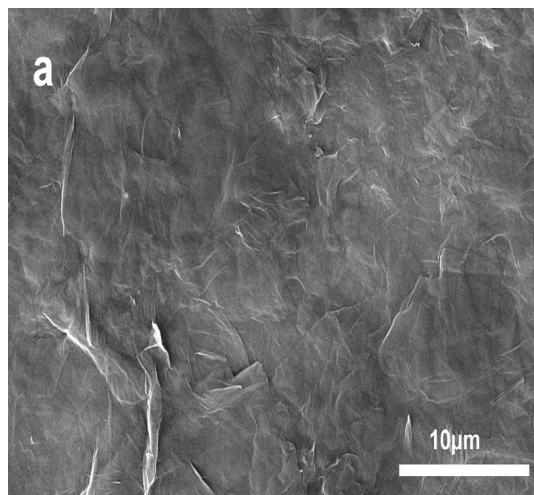


Fig. 1. SEM images of GO (a), HPW (b) and HPW-3RGO (c).

3.1.3. FTIR analysis

In order to obtain the information about functional group of the samples as well as reduction of GO to RGO in HPW-RGO during hydrothermal reaction. The FTIR of GO,

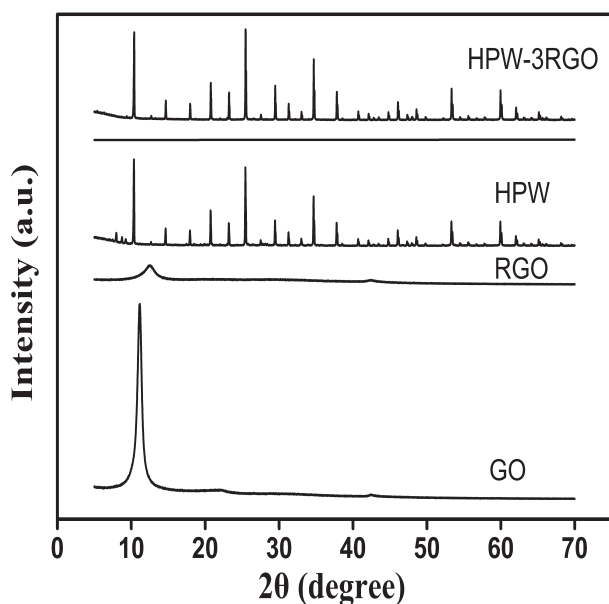


Fig. 2. XRD patterns of GO, RGO, HPW and HPW-3RGO.

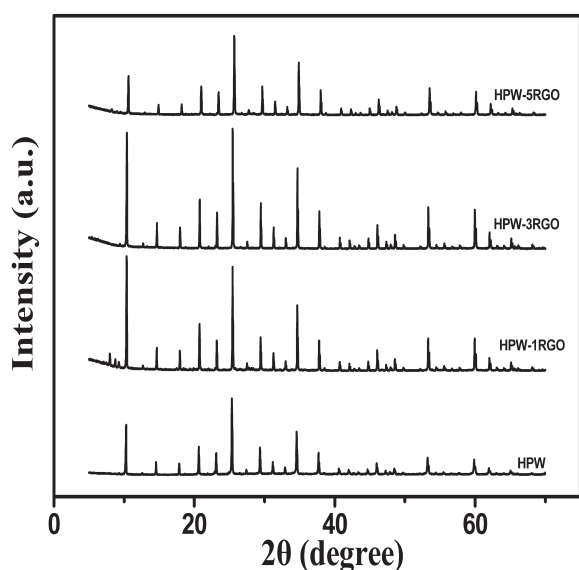


Fig. 3. XRD patterns of HPW, HPW-1RGO, HPW-2RGO and HPW-3RGO.

RGO, HPW, HPW-1RGO and HPW-3RGO materials were measured and are shown in Fig. 4. It was clear that GO had many absorption peaks corresponding to various containing oxygen functional groups, such as water O–H bending and C–C stretching ($1,646\text{ cm}^{-1}$), C–O stretching ($1,084\text{ cm}^{-1}$), C–O stretching of ether group ($1,113\text{ cm}^{-1}$) and C–O stretching of epoxide (863 cm^{-1}). The spectra of RGO showed a low absorption-peak intensity of the containing oxygen functional groups at $500\text{--}1,700\text{ cm}^{-1}$ compared with those of GO, which indicated that GO had been reduced to RGO greatly during hydrothermal process. The IR peaks of HPW were $1,073\text{ cm}^{-1}$ for $\nu\text{P-O}_a$, 987 cm^{-1} for $\nu\text{W} = \text{O}_a$, 885 cm^{-1}

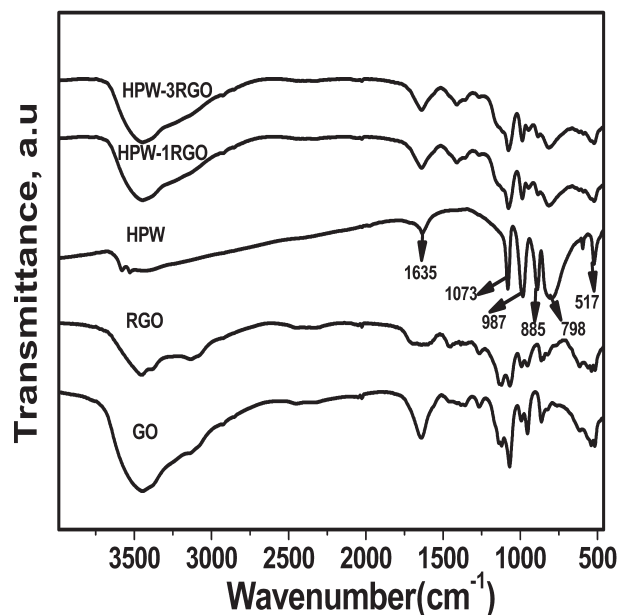


Fig. 4. The Fourier-transform infrared spectra of GO, RGO, HPW, HPW-1RGO and HPW-3RGO materials.

for $\nu\text{W-O}_b\text{-W}$ and 798 cm^{-1} for $\nu\text{W-O}_c\text{-W}$. Moreover, weaker peaks were present at 596 and 517 cm^{-1} [23], which were the characteristic of the $\text{PW}_{12}\text{O}_{40}^{3-}$ ion (Keggin ion unit). As for the FTIR spectra of HPW-RGO composites, the infrared peaks at 987 , 885 , 798 , 596 and 517 cm^{-1} were ascribed to HPW, and the peak at $1,400\text{ cm}^{-1}$ of the composites can be seen obviously from IR spectra of RGO, which indicated that the prepared composites were composed of RGO and HPW.

3.1.4. XPS analysis

In order to further investigate the chemical composition and element chemical states of HPW-RGO, XPS measurements for GO and HPW-3RGO materials were performed and the results are shown in Fig. 5. According to the XPS survey spectra (Fig. 5(a)), the HPW-3RGO material contained W, O, P and C elements corresponding to the binding energies of $\text{W}4p$, $\text{W}4d$, $\text{O}1s$, $\text{P}2s$, $\text{P}2p$ and $\text{C}1s$. Fig. 5(b) is the $\text{C}1s$ spectra comparison of GO and HPW-3RGO, the main $\text{C}1s$ peaks for GO located at 286.7 and 284.8 eV , the peak located at 286.7 eV implied that the GO contained large amount of oxygen-containing groups, HPW-RGO had much weaker obviously at 286.7 eV , which indicated that the GO was transformed to graphene greatly via hydrothermal treatment. The characteristic peaks of GO in the deconvoluted $\text{C}1s$ region appeared at 284.7 , 286.7 and 289.0 eV , which were assigned to the C–C/C=C/C–H, C=O and C(O)O functional groups, respectively [24]. Compared with $\text{C}1s$ deconvolution spectra of GO, $\text{C}1s$ deconvolution spectra peaks of HPW-3RGO existed at 284.71 and 287.12 eV (Fig. 6(d)), which were ascribed to C–C/C=C/C–H and C=O. Moreover, the peak intensity of C=O of HPW-3RGO was much weaker than that of GO. The above XPS analysis results showed that the HPW-RGO material was successfully prepared and the GO had been reduced to RGO by ethanol in the hydrothermal environment largely.

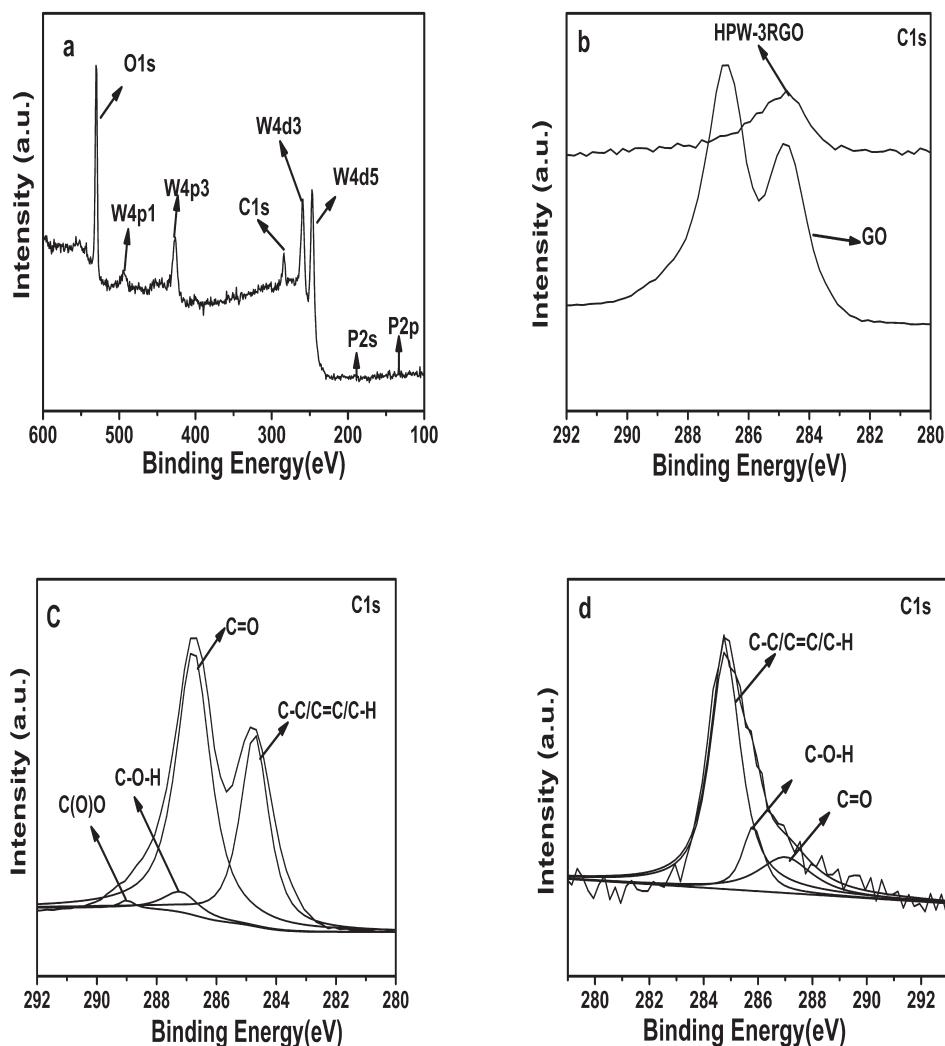


Fig. 5. (a) XPS survey spectra of HPW-3RGO; (b) C1s spectra comparison of GO and HPW-3RGO; (c) peak deconvolution of the C1s XPS core-level spectra from GO and (d) HPW-3RGO.

3.1.5. Thermogravimetric analysis

In order to investigate the thermal stability of HPW-3RGO, thermogravimetric analysis was done. Fig. 6 shows the TGA, differential scanning calorimetry (DSC) and derivative thermogravimetry (DTG) curves of HPW and HPW-3RGO hybrid composite heated in a thermal gravimetric analyzer to 700°C at a heating rate 20°C min⁻¹ under N₂ environment. The weight loss of HPW at 20°C–60°C, 60°C–210°C and 210°C–520°C were ascribed to the adsorbed water and crystal water in HPW, and the weight loss ratios were 2.74, 2.92 and 2.65 wt%, respectively. As for HPW-3RGO, the weight loss of HPW at 20°C–250°C and 260°C–600°C was also ascribed to the adsorbed water and crystal water in HPW-3RGO composite. The weight loss ratios were 5.14 and 3.17 wt%, respectively. Comparing weight loss ratios of HPW and HPW-3RGO, HPW-3RGO had much more weight loss ratio because oxygen-containing groups of RGO may be reduced under thermal environment (over 250°C) [25]. Moreover, from the DSC curves of them, crystal phase change of both HPW and HPW-3RGO occurred over 600°C.

3.2. Adsorption and photocatalytic performance

3.2.1. The optimization of RGO amount in HPW-RGO nanocomposites

To investigate the effect of RGO amount in HPW-RGO composites on the removal ratios of MO, the adsorption and photocatalytic degradation of MO over HPW-1RGO, HPW-3RGO, HPW-5RGO composites was carried out and is shown in Fig. 7(a). Fig. 7(a) shows that the adsorption removal ratios of MO on the HPW-1RGO, HPW-3RGO and HPW-5RGO were 27.81%, 30.86% and 35.20%, respectively. The adsorption removal ratio of MO over HPW-RGO composites increased from 27.81% to 35.20% with the increasing weight ratio of RGO from 1 to 5 wt% in the composites. The enhanced adsorption ability could be attributed to the π - π interaction strong and hydrogen bonds between RGO and pollutants containing phenyl group, which was in consistent with the result of Xu et al. [14]. The introduction of RGO to HPW via hydrothermal reaction exhibited a significant influence on the adsorption ability for MO. After light

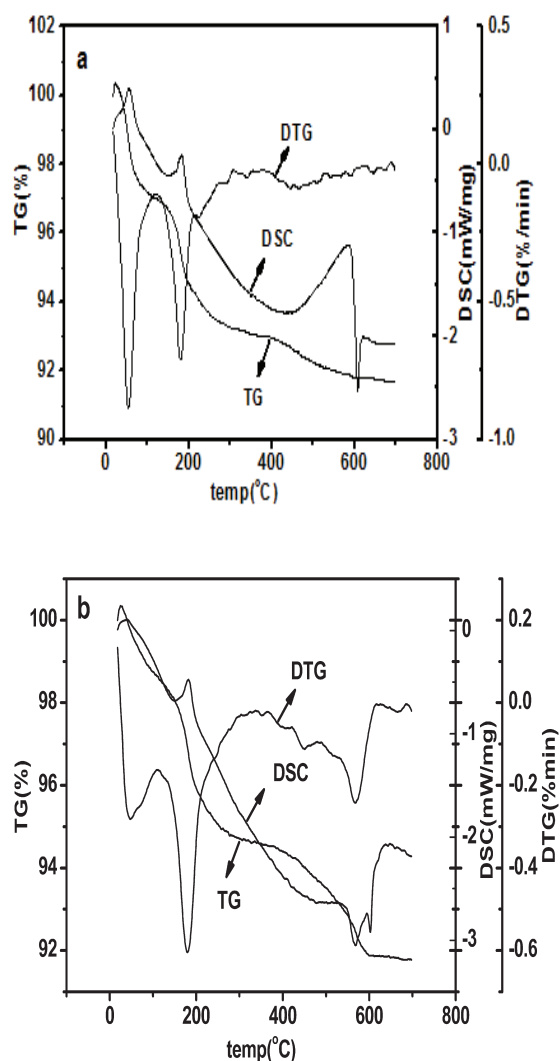


Fig. 6. TGA, DSC and DTG curves of HPW (a) and HPW-3RGO (b).

illumination, photocatalytic degradation removal ratios of MO on HPW-1RGO, HPW-3RGO and HPW-5RGO were 33.90%, 38.68% and 38.24%, respectively. The HPW-3RGO had highest degradation removal ratio. The total removal ratio of MO over HPW-1RGO, HPW-3RGO and HPW-5RGO were 61.71%, 69.54% and 73.44%, respectively. In order to assess the photocatalytic activities of them, the pseudo-first-order degradation kinetic constants for MO over the HPW-1RGO, HPW-3RGO and HPW-5RGO were 0.00416, 0.00583 and 0.0064 min^{-1} , respectively (Fig. 7(b)). It was evident that the degradation rate constant of MO enhanced greatly ranging from 0.00416 to 0.00583 min^{-1} with increasing mass ratio of RGO from 1 to 3 wt%. Further increasing the RGO amount from 3 to 5.0 wt%, the degradation rate constant only increased slightly from 0.00583 to 0.0064 min^{-1} . This demonstrated that much more RGO did not help to improve photocatalytic activity of HPW greatly because higher RGO content will make the light absorption weak. Therefore, from the both view of photocatalytic degradation removal ratio and economical point, the optimal content of RGO in composite was selected 3.0 wt%.

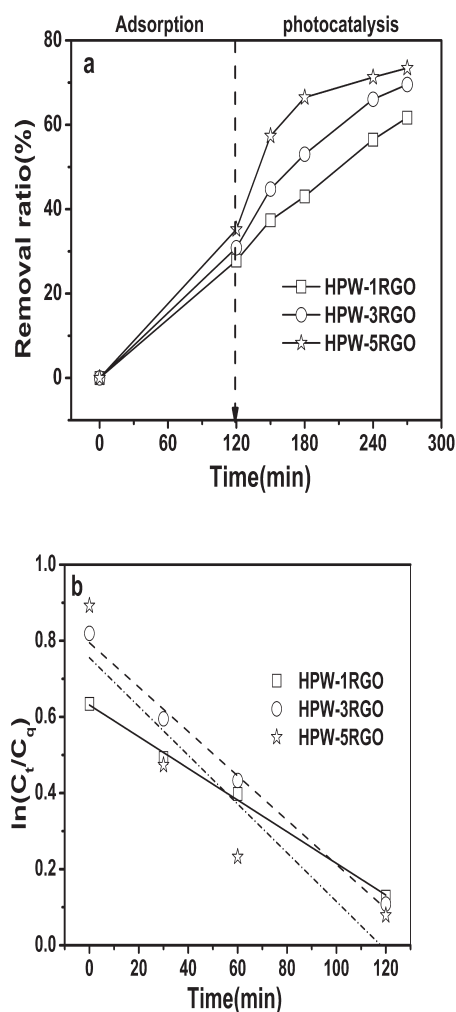


Fig. 7. (a) Adsorption and photocatalytic decomposition time courses of MO (initial concentration 20 mg/L) on HPW-1RGO, HPW-3RGO and HPW-5RGO nanocomposites (catalyst dosage 0.6 g/L) and (b) the corresponding first-order plots. The arrow indicates the beginning of UV light irradiation.

3.2.3. The photocatalytic performance evaluation of HPW-3RGO

In order to contribution of RGO in composites to MO removal ratio, the adsorption and decomposition time courses of MO over HPW-3RGO, HPW and photolysis of MO were performed and are shown in Fig. 8. The experiment condition was 20 mg/L MO, 1.0 g/L photocatalyst and pH 3.0 of solution. From Fig. 8(a) we can see the adsorption removal ratio of MO over HPW-RGO was 46.34%, the photocatalytic degradation removal ratio was about 40.00%, and the total removal ratio was 86.34%. The adsorption removal ratio of MO over HPW was 2.67%, the photocatalytic degradation removal ratio was about 32.00% and the total removal ratio was only 34.66%. The introduced RGO made a great contribution to the RGO removal. The degradation rate constant of HPW-RGO (0.00892 min^{-1}) was 3.4 times of the HPW (0.00264 min^{-1}), and the rate constant of photolysis was only 0.000792 min^{-1} (Fig. 8(b)).

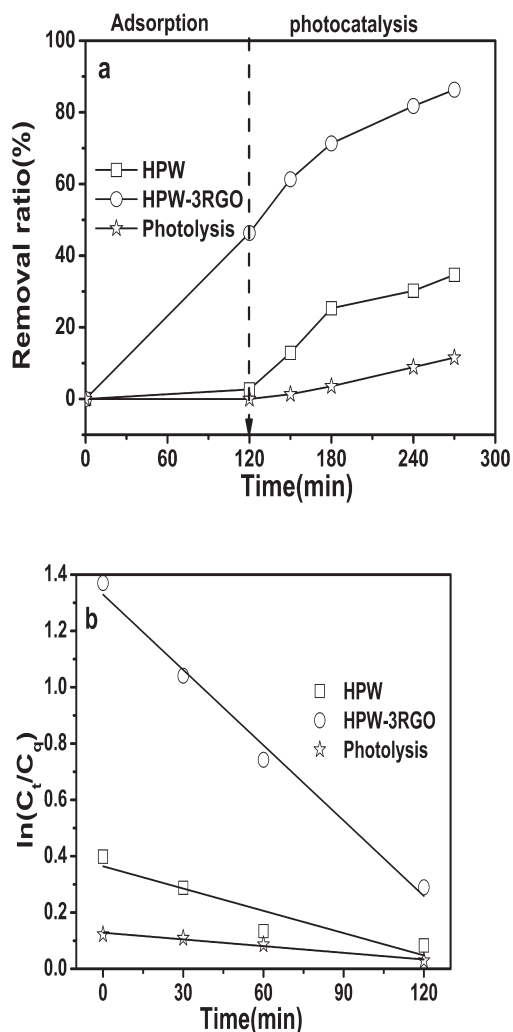


Fig. 8. (a) Direct photolysis (20 W UV light, main wavelength 254 nm) and adsorption and photocatalytic decomposition time courses of MO (initial concentration 20 mg/L) on HPW-3RGO and HPW (catalyst dosages 1.0 g/L) and (b) the corresponding first-order plots. The arrow indicates the beginning of UV light irradiation.

Based on the above experimental data analysis, we can know that HPW-3RGO had much better adsorption ability for MO and better photocatalytic activity compared with pure HPW because RGO can absorb MO from water to the surface of HPW-3RGO through strong π - π interaction between RGO and two phenyl groups of MO, then adsorbed MO can be decomposed. In addition, improvement of photocatalytic degradation rate of MO over HPW-3RGO was that RGO in composites maybe suppress the combination of photogenerated electron-hole pairs due to its excellent electron conductivity [26].

4. Conclusions

In summary, HPW-RGO composites were synthesized by hydrothermal method. The morphology and

crystal phase structure, chemical composition of prepared HPW-RGO were investigated in detail. The RGO mass ratios in HPW-RGO composites were optimized by removing MO. The results indicated that the HPW was dispersed on RGO sheet, and the optimal RGO mass ratio in composites was 3.0 wt%. Under experiment condition (1.0 g/L dosage, pH 3.0 and 20 mg/L MO solution), the adsorption removal ratio of MO over HPW-RGO was 46.34%, the photocatalytic degradation removal ratio is about 40.00%, and the total removal ratio was 86.34%. The adsorption removal ratio of MO over HPW was 2.67%, the photocatalytic degradation removal ratio is about 32.00%, and the total removal ratio was only 34.66%. The degradation rate constant of HPW-RGO (0.00892 min^{-1}) was 3.4 times of the HPW (0.00264 min^{-1}). The results showed that RGO played a dominant role in enhancing the adsorption ability and photocatalytic activity of the HPW-RGO for the MO removal. It is feasible and efficient to remove MO and other organic pollutants over the prepared HPW-RGO composites by adsorption and photocatalysis.

Acknowledgments

This work was financially supported by the Natural Science Foundation of China (No. 21767030), Natural Science Foundation of Yunnan Province (2016FB014) and Foundation of Education Bureau of Yunnan Province (2017ZZX087).

References

- [1] K. Hashimoto, H. Irie, A. Fujishima, TiO_2 photocatalysis: a historical overview and future prospects, *JPN. J. Appl. Phys. Part 1: Regular Papers, Brief Commun., Rev. Papers* 44 (2005) 8269–8285.
- [2] K. Nakata, A. Fujishima, TiO_2 photocatalysis: design and applications, *J. Photochem. Photobiol., C*, 13 (2012) 169–189.
- [3] C.G. Feng, Y.Z. Li, X. Liu, Photocatalytic degradation of imidacloprid by phosphotungstic acid supported on a mesoporous sieve MCM-41, *Chin. J. Chem.*, 30 (2012) 127–132.
- [4] M.A. Schwegler, P. Vinke, M. Van der Eijk, H. Van Bekkum, Activated carbon as a support for heteropolyanion catalysts, *Appl. Catal., A*, 80 (1992) 41–57.
- [5] L. Zhao, Y. Chi, Q. Yuan, N. Li, W.F. Yan, X.T. Li, Phosphotungstic acid anchored to amino-functionalized core-shell magnetic mesoporous silica microspheres: a magnetically recoverable nanocomposite with enhanced photocatalytic activity, *J. Colloid Interface Sci.*, 390 (2013) 70–77.
- [6] S.Y. Tao, Y.C. Wang, Y.X. Yu, Y.L. An, W.P. Shi, Hierarchically porous tungstophosphoric acid/silica hybrid for high performance vis-light photocatalysis, *J. Environ. Chem. Eng.* 1 (2013) 719–727.
- [7] J. Thomas, S. Radhika, M.J. Yoon, Nd^{3+} -doped TiO_2 nanoparticles incorporated with heteropoly phosphotungstic acid: a novel solar photocatalyst for degradation of 4-chlorophenol in water, *J. Mol. Catal., A*, 411 (2016) 146–156.
- [8] Q. Deng, W.H. Zhou, X.M. Li, Z.S. Peng, S.L. Jiang, M. Yue, T.J. Cai, Microwave radiation solid-phase synthesis of phosphotungstate nanoparticle catalysts and photocatalytic degradation of formaldehyde, *J. Mol. Catal., A*, 262 (2007) 149–155.
- [9] K. Sapiro, Y. Ide, T. Sano, M. Sadakane, One-pot synthesis of microporous and mesoporous $(\text{NH}_4)_3\text{PW}_{12}\text{O}_{40}$ by reaction of in-situ generated $\text{PW}_{12}\text{O}_{40}^{3-}$ with NH_4^+ in a strongly acidic solution, *Mater. Res. Bull.*, 48 (2013) 4157–4162.
- [10] T.H. Li, Q.G. Li, J.Y. Yan, F. Li, Photocatalytic degradation of organic dyes by $\text{La}^{3+}/\text{Ce}^{3+}$ - $\text{H}_3\text{PW}_{12}\text{O}_{40}$ under different light irradiation, *Dalton Trans.*, 43 (2014) 9061–9069.

- [11] C.N.R. Rao, A.K. Sood, K.S. Subrahmanyam, A. Govindaraj, Graphene: the new two-dimensional nanomaterial, *Angew. Chem. Int.*, 48 (2009) 7752–7777.
- [12] J.C. Meyer, A.K. Geim, M.I. Katsnelson, K.S. Novoselov, T.J. Booth, S. Roth, The structure of suspended graphene sheets, *Nature*, 446 (2007) 60–63.
- [13] T.V. Khai, D.S. Kwak, Y.J. Kwon, H.Y. Cho, T.N. Huan, H. Chung, H. Ham, C. Lee, N.V. Dan, N.T. Tung, H.W. Kim, Direct production of highly conductive graphene with a low oxygen content by a microwave-assisted solvothermal method, *Chem. Eng. J.*, 232 (2013) 346–355.
- [14] J. Xu, L. Wang, Y. Zhu, Decontamination of bisphenol A from aqueous solution by graphene adsorption, *Langmuir* 28 (2012) 8418–8425.
- [15] H. Zhang, X.J. Lv, Y.M. Li, Y. Wang, J.H. Li, P25-graphene composite as a high performance photocatalyst, *ACS Nano*, 4 (2010) 380–386.
- [16] Y.H. Zhang, Z.R. Tang, X.Z. Fu, Y.J. Xu, TiO₂-graphene nanocomposites for gas-phase photocatalytic degradation of volatile aromatic pollutant: is TiO₂-graphene truly different from other TiO₂-carbon composite materials? *ACS Nano*, 4 (2010) 7303–7314.
- [17] Y.H. Yang, E.Z. Liu, H.Z. Dai, L.M. Kang, H.T. Wu, J.F. Fan, X.Y. Hu, H.C. Liu, Photocatalytic activity of Ag-TiO₂-graphene ternary nanocomposites and application in hydrogen evolution by water splitting, *Int. J. Hydrogen Energy*, 39 (2014) 7664–7671.
- [18] Q.J. Xiang, J.G. Yu, M. Jaroniec, Synergetic effect of MoS₂ and graphene as cocatalysts for enhanced photocatalytic H₂ production activity of TiO₂ nanoparticles, *J. Am. Chem. Soc.*, 134 (2012) 6575–6578.
- [19] S. William, W.S. Hummers, Preparation of graphitic oxide, *J. Am. Chem. Soc.*, 80 (1958) 1339–1339.
- [20] S. Stankovich, D.A. Dikin, G.H.B. Dommett, K.M. Kohlhaas, E.J. Zimney, E.A. Stach, R.D. Piner, S.T. Nguyen, R.S. Ruoff, Graphene-based composite materials, *Nature*, 442 (2006) 282–286.
- [21] Y.H. Zhang, Z. R. Tang, X.Z. Fu, Y.J. Xu, TiO₂-graphene nanocomposites for gas-phase photocatalytic degradation of volatile aromatic pollutant: is TiO₂-graphene truly different from other TiO₂-carbon composite materials? *ACS Nano*, 4 (2010) 7303–7314.
- [22] S.D. Perera, R.G. Mariano, K. Vu, N. Nour, O. Seitz, Y. Chabal, K.J. Balkus, Hydrothermal synthesis of graphene-TiO₂ nanotube composites with enhanced photocatalytic activity, *ACS Catal.*, 2 (2012) 949–956.
- [23] D. Huang, Y.J. Wang, L.M. Yang, G.S. Luo, Direct synthesis of mesoporous TiO₂ modified with phosphotungstic acid under template-free condition, *Micropor. Mesopor. Mater.*, 96 (2006) 301–306.
- [24] E. Lee, J.Y. Hong, H. Kang, J. Jang, Synthesis of TiO₂ nanorod-decorated graphene sheets and their highly efficient photocatalytic activities under visible-light irradiation, *J. Hazard. Mater.*, 219–220 (2012) 13–18.
- [25] W.L. Zhang, H.J. Choi, Silica-graphene oxide hybrid composite particles and their electroresponsive characteristics, *Langmuir*, 28 (2012) 7055–7062.
- [26] Y. Yan, S.F. Sun, Y. Song, X. Yan, W.S. Guan, X.L. Liu, W.D. Shi, Microwave-assisted in situ synthesis of reduced graphene oxide-BiVO₄ composite photocatalysts and their enhanced photocatalytic performance for the degradation of ciprofloxacin, *J. Hazard. Mater.*, 250–251 (2013) 106–114.